

Multiconfiguration Dirac-Hartree-Fock calculations of atomic electric dipole moments of ^{225}Ra , ^{199}Hg , and ^{171}Yb

Laima Radžiūtė,¹ Gediminas Gaigalas,¹ Per Jönsson,² and Jacek Bieroń³¹*Vilnius University, Institute of Theoretical Physics and Astronomy, A. Goštauto 12, LT-01108 Vilnius, Lithuania*²*Group for Materials Science and Applied Mathematics, Malmö University, S-20506 Malmö, Sweden*³*Instytut Fizyki imienia Mariana Smoluchowskiego, Uniwersytet Jagielloński, Kraków, Poland*

(Received 30 December 2013; published 30 July 2014)

The multiconfiguration Dirac-Hartree-Fock method is employed to calculate atomic electric dipole moments in the ground states of ^{225}Ra , ^{199}Hg , and ^{171}Yb . For the calculations of the matrix elements we extend the relativistic atomic structure package GRASP2K. The extension includes programs to evaluate matrix elements of \mathcal{PT} -odd electron-nucleus tensor-pseudotensor and pseudoscalar-scalar interactions, the atomic electric dipole operator, the nuclear Schiff moment, and the interaction of the electron electric dipole moment with nuclear magnetic moments. The interelectronic interactions are accounted for through valence and core-valence electron correlation effects. The electron shell relaxation is included with separately optimized wave functions of opposite parities.

DOI: [10.1103/PhysRevA.90.012528](https://doi.org/10.1103/PhysRevA.90.012528)

PACS number(s): 32.10.Dk, 11.30.Er, 31.15.A–, 24.80.+y

I. INTRODUCTION

The existence of a nonzero permanent electric dipole moment (EDM) of an elementary particle or a composite system of particles would violate time-reversal symmetry (\mathcal{T}), as well as the combined charge conjugation and parity symmetry (\mathcal{CP}), due to the \mathcal{CPT} theorem [1]. One of the principal motivations behind the experimental searches of EDMs is to shed light on the observed matter-antimatter asymmetry in the universe, which in turn is linked to an asymmetry in the Big Bang baryon-antibaryon production. The standard model of elementary particles cannot explain the matter-antimatter asymmetry in the universe, as the standard model predicts sources of \mathcal{CP} violation (and of EDMs) several orders of magnitude weaker than those needed to account for the observed baryon numbers. This leads to proliferation of the extensions to the standard model. Some of these extensions predict larger EDMs, sometimes within the reach of current experiments. The experimental searches have not yet detected a nonzero EDM, but they continue to improve the limits on EDMs of individual elementary particles, as well as limits on \mathcal{CP} -violating interactions, usually parametrized by the interaction constants C_T and C_P (see Sec. II for details and Table II in Ref. [2] for a summary). These limits constrain the theoretical extensions of the standard model of elementary particles. In recent years these constraints have been set by the measurements of EDMs of neutrons [3], electrons in a paramagnetic atom (a thallium atom experiment [4]), electrons in a diamagnetic atom (mercury atom [2]), and in TlF and YbF molecules [5,6]. The search for EDMs is not restricted to the above species though; see, e.g., [7,8].

The search for a permanent electric dipole moment of an elementary particle, or a composite system of particles (see [1], or Ref. [9] for a recent review), is a challenge not only for experiments, but also for theories of composite systems. Heavy atoms are excellent examples of composite systems with large EDMs due to the existence of mechanisms that may induce atomic EDMs several orders of magnitude larger than an intrinsic particle EDM. In the present paper we computed the EDMs in the ground states of three diamagnetic atoms

^{225}Ra , ^{199}Hg , and ^{171}Yb . The purpose of the present paper is fourfold. First, we test the recently developed programs to evaluate matrix elements of \mathcal{PT} -odd electron-nucleus (e - N) tensor-pseudotensor and pseudoscalar-scalar interactions, the atomic electric dipole operator, the nuclear Schiff moment, and the interaction of the electron electric dipole moment with nuclear magnetic moments. Second, we generate the atomic wave functions in several different approaches in order to test the dependence of the calculated atomic EDMs on options available in the GRASP2K [10] implementation of the multiconfiguration Dirac-Hartree-Fock (MCDHF) method. The approaches depend on the choice of variational energy functional (average level versus optimal level, with different numbers of optimized levels), the choice of wave functions built on a common orbital set or several separately optimized orbital sets (in the latter case biorthogonal transformations of wave functions had to be applied), and specific methods of one-electron orbital generation. All these approaches are discussed in more detail in Secs. III B–III E and presented in Tables I–III. Third, we sequentially generate several layers of virtual (correlation) orbitals for each of the three elements and observed the effects of electron correlation on atomic EDMs. All valence and core-valence electron correlation effects are included through single and restricted double electron substitutions from core and valence shells to virtual orbitals. Finally, we provide independently calculated atomic EDMs in the $J = 0$ ground states of ^{225}Ra , ^{199}Hg , and ^{171}Yb and compare our results with those of other authors. Our results, presented in Tables IV–VII, are obtained within the MCDHF method, using the relativistic atomic structure package GRASP2K [10], which, in addition to one paper [11] on the Schiff moment in radium, has been employed in the calculations of matrix elements of \mathcal{PT} -odd e - N tensor-pseudotensor and pseudoscalar-scalar interactions, the nuclear Schiff moment, and the interaction of the electron electric dipole moment with nuclear magnetic moments. (Preliminary results of these calculations were presented in [12].)

The three atoms ^{225}Ra , ^{199}Hg , and ^{171}Yb have been chosen on the grounds that they have similar valence shell structure.

All these elements are diamagnetic, with a closed outer s shell ($^{225}\text{Ra } 6p^67s^2$, $^{199}\text{Hg } 5d^{10}6s^2$, and $^{171}\text{Yb } 4f^{14}6s^2$). In the future we will be able to extend these calculations to closed- p -valence-shell atoms, as well as to any other closed- or open-shell system. Our current MCDHF machinery [10] is robust enough to deal with electron correlation effects in arbitrary atomic systems, including the lanthanides and actinides.

II. EDM THEORY

This section is based on the review by Ginges and Flambaum [7]. We present here only the expressions for the four \mathcal{PT} -odd operators described in Sec. I above, and the corresponding matrix elements necessary for the discussion of the results. The reader is referred to the review in [7] for full explanations and to [13] for the explicit form of the matrix elements (the only difference is the prefactor $1/r$, which is absorbed in the definition of radial wave functions).

The interactions that mix atomic states of different parities and induce a static electric dipole moment of an atom are quite weak. Therefore, an atomic state function (ASF) of a mixed-parity state can be expressed as

$$\tilde{\Psi}(JM_J) = a\Psi(\gamma PJM_J) + \sum_i b_i\Psi(\gamma_i(-P)J_iM_{J_i}), \quad (1)$$

where the coefficient a of the dominant contribution can be set to 1. The expansion coefficients of opposite-parity ($-P$) admixtures b_i can be found using first-order perturbation theory

$$b_i = \frac{\langle\Psi(\gamma_i(-P)J_iM_{J_i})|\hat{H}_{\text{int}}|\Psi(\gamma PJM_J)\rangle}{E(\gamma PJ) - E(\gamma_i(-P)J_i)}, \quad (2)$$

where \hat{H}_{int} represents the Hamiltonian of the \mathcal{PT} -odd interaction, which mixes states of opposite parities. The mixed-parity state of a particular atomic level $^{2S+1}L_J$ induces a static EDM of an atom

$$\begin{aligned} d_{\text{at}}^{\text{int}} &= \langle\tilde{\Psi}(\gamma JM_J)|\hat{D}_z|\tilde{\Psi}(\gamma JM_J)\rangle \\ &= 2 \sum_i b_i \langle\Psi(\gamma PJM_J)|\hat{D}_z|\Psi(\gamma_i(-P)J_iM_{J_i})\rangle, \end{aligned} \quad (3)$$

where \hat{D}_z represents the z projection of the electric dipole moment operator. Eventually, an atomic EDM can be written as a sum

$$d_{\text{at}}^{\text{int}} = 2 \sum_i \frac{\langle 0|\hat{D}_z|i\rangle\langle i|\hat{H}_{\text{int}}|0\rangle}{E_0 - E_i}, \quad (4)$$

where $|0\rangle$ represents the ground state $|\Psi(\gamma PJM_J)\rangle$, with $J = 0$ and even parity, and the summation runs over excited states $|\Psi(\gamma_i(-P)J_iM_{J_i})\rangle$, with $J_i = 1$ and odd parity. Here E_0 and E_i are energies of ground and excited states, respectively. In practice, this sum needs to be truncated at some level. Calculations of atomic EDMs require evaluation of the matrix element of the static EDM $\langle 0|\hat{D}_z|i\rangle$ and the matrix element of the interactions that induced EDMs in an atom $\langle i|\hat{H}_{\text{int}}|0\rangle$. The operators associated with the above matrix elements are all one-particle operators.

For the general tensor operator \hat{T}_q^k , the matrix element between states of different parity can be expressed by the

Wigner-Eckart theorem as

$$\begin{aligned} &\langle\Psi(\gamma PJM_J)|\hat{T}_0^k|\Psi(\gamma_i(-P)J_iM_{J_i})\rangle \\ &= (-1)^{J-M_J} \sqrt{2J+1} \begin{pmatrix} J & k & J_i \\ -M_J & 0 & M_{J_i} \end{pmatrix} \\ &\quad \times [\Psi(\gamma PJ)\|\hat{T}^k\|\Psi(\gamma_i(-P)J_i)]. \end{aligned} \quad (5)$$

Expanding the wave functions in configuration state functions (CSFs) $\Phi(\gamma PJ)$ that are built from one-electron Dirac orbitals (see Sec. III), the reduced matrix elements of \hat{T}_q^k can be written

$$\begin{aligned} &[\Psi(\gamma PJ)\|\hat{T}^k\|\Psi(\gamma_i(-P)J_i)] \\ &= \sum_{r,s} c_r c_s [\Phi(\gamma_r PJ)\|\hat{T}^k\|\Phi(\gamma_s(-P)J_i)], \end{aligned} \quad (6)$$

where c_r and c_s are mixing coefficients of CSFs (even and odd parity, respectively). The matrix elements between the CSFs in turn can be written as sums of single-particle matrix elements

$$[\Phi(\gamma_r PJ)\|\hat{T}^k\|\Phi(\gamma_s(-P)J_i)] = \sum_{a,b} d_{ab}^k(rs) [n_a \kappa_a \|\hat{t}^k\| n_b \kappa_b]. \quad (7)$$

In the latter expansion, the $d_{ab}^k(rs)$ are known as spin angular coefficients that arise from using Racah's algebra in the decomposition of the many-electron matrix elements [14,15]. Expressions (5)–(7) are general and can be used for any one-particle operator.

We consider the following four mechanisms that may induce atomic EDMs: tensor-pseudotensor (TPT) interaction \hat{H}_{TPT} , pseudoscalar-scalar (PSS) interaction \hat{H}_{PSS} , Schiff moment (SM) interaction \hat{H}_{SM} , and the electron EDM interaction with the nuclear magnetic field \hat{H}_B . The interactions, which are all of rank $k = 1$, are discussed in more detail in the following sections. In addition, the expression for the electric dipole interaction is given.

A. Electric dipole operator

The electric dipole moment operator has the rank $k = 1$ in (5)–(7) and the single-particle reduced matrix element $[n_a \kappa_a \|\hat{t}^k\| n_b \kappa_b]$ in Eq. (7) can be written as

$$[n_a \kappa_a \|\hat{d}^1\| n_b \kappa_b] = -[\kappa_a \|C^1\| \kappa_b] \int_0^\infty (P_a P_b + Q_a Q_b) r dr, \quad (8)$$

where P and Q are large and small components of the relativistic radial wave functions, respectively. The single-particle angular reduced matrix elements can be expressed as

$$\begin{aligned} [\kappa_a \|C^k\| \kappa_b] &= (-1)^{j_a+1/2} \sqrt{2j_b+1} \\ &\quad \times \begin{pmatrix} j_a & k & j_b \\ 1/2 & 0 & -1/2 \end{pmatrix} \pi(l_a, l_b, k), \end{aligned} \quad (9)$$

where $\pi(l_a, l_b, k)$ is defined as

$$\pi(l_a, l_b, k) = \begin{cases} 1 & \text{for } l_a + k + l_b \text{ even} \\ 0 & \text{otherwise.} \end{cases} \quad (10)$$

B. Tensor-pseudotensor interaction

One of the possible sources of the EDM in diamagnetic atoms is the tensor-pseudotensor interaction between electrons and nucleons, violating both parity and time-reversal invariance. It can be expressed as [1,7]

$$\hat{H}_{\text{TPT}} = i\sqrt{2}G_F C_T \sum_{j=1}^N \langle \sigma_A \cdot \boldsymbol{\gamma}_j \rangle \rho(r_j), \quad (11)$$

where G_F is the Fermi coupling constant, A is the number of nucleons, γ_j is the Dirac matrix, and C_T is a dimensionless coupling constant of the TPT interaction and is equal to zero within the standard model, but is finite in some theories beyond the standard model of elementary particle physics. According

to Dzuba *et al.* [13],

$$C_T \langle \sigma_A \rangle = \left\langle C_T^p \sum_p \sigma_p + C_T^n \sum_n \sigma_n \right\rangle, \quad (12)$$

where $\langle \dots \rangle$ represents averaging over the nuclear state with the nuclear spin I . The nuclear charge density distribution $\rho(r)$ is the normalized to unity two-component Fermi function [16]

$$\rho(r) = \frac{\rho_0}{1 + e^{(r-b)/a}}, \quad (13)$$

where a and b depend on the mass of the isotope. The single-particle reduced matrix element $[n_a \kappa_a \| \hat{t}^k \| n_b \kappa_b]$ in Eq. (7) for the tensor-pseudotensor interaction has the form

$$\begin{aligned} [n_a \kappa_a \| \hat{h}_{\text{TPT}}^1 \| n_b \kappa_b] &= \sqrt{2} G_F C_T \langle \sigma_A \rangle [n_a \kappa_a \| i \hat{\gamma}^1 \rho(r) \| n_b \kappa_b] \\ &= -\sqrt{2} G_F C_T \langle \sigma_A \rangle \left([-\kappa_a \| \sigma^1 \| \kappa_b] \int_0^\infty P_b Q_a \rho(r) dr + [\kappa_a \| \sigma^1 \| -\kappa_b] \int_0^\infty P_a Q_b \rho(r) dr \right), \end{aligned} \quad (14)$$

where the single-particle angular reduced matrix elements can be expressed as

$$[-\kappa_a \| \sigma^1 \| \kappa_b] = \frac{\langle l_b \frac{1}{2} 0 \frac{1}{2} | j_a \frac{1}{2} \rangle \langle l_b \frac{1}{2} 0 \frac{1}{2} | j_b \frac{1}{2} \rangle - \langle l_b \frac{1}{2} 1 -\frac{1}{2} | j_a \frac{1}{2} \rangle \langle l_b \frac{1}{2} 1 -\frac{1}{2} | j_b \frac{1}{2} \rangle}{\langle j_b 1 \frac{1}{2} 0 | j_a \frac{1}{2} \rangle}, \quad (15)$$

$$[\kappa_a \| \sigma^1 \| -\kappa_b] = \frac{\langle l_a \frac{1}{2} 0 \frac{1}{2} | j_a \frac{1}{2} \rangle \langle l_a \frac{1}{2} 0 \frac{1}{2} | j_b \frac{1}{2} \rangle - \langle l_a \frac{1}{2} 1 -\frac{1}{2} | j_a \frac{1}{2} \rangle \langle l_a \frac{1}{2} 1 -\frac{1}{2} | j_b \frac{1}{2} \rangle}{\langle j_b 1 \frac{1}{2} 0 | j_a \frac{1}{2} \rangle}. \quad (16)$$

C. Pseudoscalar-scalar interaction

The interaction Hamiltonian for the pseudoscalar-scalar interaction between the electrons and the nucleus reads [1,7]

$$\hat{H}_{\text{PSS}} = \frac{-G_F C_P}{2\sqrt{2}m_p c} \sum_{j=1}^N \gamma_0 (\nabla_j \rho(r_j)) \langle \sigma_A \rangle, \quad (17)$$

where C_P is dimensionless coupling constant of the PSS interaction. Analogously to the TPT interaction, the constant C_P is zero within the standard model. According to Dzuba *et al.* [13],

$$C_P \langle \sigma_A \rangle = \left\langle C_P^p \sum_p \sigma_p + C_P^n \sum_n \sigma_n \right\rangle. \quad (18)$$

The single-particle reduced matrix element $[n_a \kappa_a \| \hat{t}^k \| n_b \kappa_b]$ in Eq. (7) for the pseudoscalar-scalar interaction has the form

$$\begin{aligned} [n_a \kappa_a \| \hat{h}_{\text{PSS}}^1 \| n_b \kappa_b] &= -\frac{G_F C_P}{2\sqrt{2}m_p c} \langle \sigma_A \rangle [n_a \kappa_a \| \gamma_0 \nabla^1 \rho(r) \| n_b \kappa_b] \\ &= -\frac{G_F C_P}{2\sqrt{2}m_p c} \langle \sigma_A \rangle [\kappa_a \| C^1 \| \kappa_b] \\ &\quad \times \int_0^\infty (P_a P_b - Q_a Q_b) \frac{d\rho(r)}{dr} dr. \end{aligned} \quad (19)$$

D. Schiff moment

The Hamiltonian of this interaction can be expressed as [7,17]

$$\hat{H}_{\text{SM}} = \frac{3}{B} \sum_{j=1}^N (\mathbf{S} \cdot \mathbf{r}_j) \rho(r_j). \quad (20)$$

The Schiff moment \mathbf{S} is directed along the nuclear spin I and $\mathbf{S} \equiv S\mathbf{I}/I$, with S being the coupling constant and $B = \int_0^\infty \rho(r)r^4 dr$. The single-particle reduced matrix element $[n_a \kappa_a \| \hat{t}^k \| n_b \kappa_b]$ in expansion (7) for the Schiff moment can be factorized into a reduced angular matrix element and a radial integral

$$\begin{aligned} [n_a \kappa_a \| \hat{h}_{\text{SM}}^1 \| n_b \kappa_b] &= \frac{3}{B} S [n_a \kappa_a \| \hat{r}^1 \rho(r) \| n_b \kappa_b] \\ &= \frac{3}{B} S [\kappa_a \| C^1 \| \kappa_b] \\ &\quad \times \int_0^\infty (P_a P_b + Q_a Q_b) \rho(r) r dr. \end{aligned} \quad (21)$$

E. Electron electric dipole moment

The operator for the electron EDM interaction with the magnetic field of a nucleus in a different form may be

expressed as [13]

$$\hat{H}_B = -id_e \sum_{j=1}^N (\boldsymbol{\gamma}_j \mathbf{B}), \quad (22)$$

where d_e represents the electron electric dipole moment and \mathbf{B} the magnetic field of the nucleus. The

$$\begin{aligned} [n_a \kappa_a \| h_B^{el} \| n_b \kappa_b] = & \frac{d_e \mu}{2m_p c} \left(-3[-\kappa_a \| C^1 \| -\kappa_b] \int_R^\infty \frac{Q_a P_b}{r^3} dr - 3[\kappa_a \| C^1 \| \kappa_b] \int_R^\infty \frac{P_a Q_b}{r^3} dr - [-\kappa_a \| \sigma^1 \| \kappa_b] \int_R^\infty \frac{Q_a P_b}{r^3} dr \right. \\ & \left. - [\kappa_a \| \sigma^1 \| -\kappa_b] \int_R^\infty \frac{P_a Q_b}{r^3} dr + 2[-\kappa_a \| \sigma^1 \| \kappa_b] \int_0^R \frac{Q_a P_b}{R^3} dr + 2[\kappa_a \| \sigma^1 \| -\kappa_b] \int_0^R \frac{P_a Q_b}{R^3} dr \right), \quad (23) \end{aligned}$$

where R and μ represent the nuclear radius and nuclear magnetic moment, respectively.

We extended the GRASP2K [10] package for the calculation of the matrix elements (7) and for the calculation of single-particle reduced matrix elements (8), (14), (19), (21), and (23). The extension, presented in this work, includes subroutines for calculation of matrix elements of type $\langle i | \hat{H}_{\text{int}} | 0 \rangle$ in Eq. (4) for the tensor-pseudotensor \hat{H}_{TPT} , pseudoscalar-scalar \hat{H}_{PSS} , Schiff moment \hat{H}_{SM} , electron EDM interaction with nuclear magnetic field \hat{H}_B , and electric dipole moment \hat{D}_z .

III. MCDHF CALCULATIONS

A. MCDHF theory

We used the MCDHF approach to generate numerical representations of atomic wave functions. An atomic state function $\Psi(\gamma P J M_J)$ is obtained as a linear combination of configuration state functions $\Phi(\gamma_r P J M_J)$, eigenfunctions of the parity P , and total angular momentum operators J^2 and M_J :

$$\Psi(\gamma P J M_J) = \sum_r c_r \Phi(\gamma_r P J M_J), \quad (24)$$

where c_r are configuration mixing coefficients. The multiconfiguration energy functional was based on the Dirac-Coulomb Hamiltonian, given (in a.u.) by

$$\hat{H}_{\text{DC}} = \sum_{j=1}^N [c \boldsymbol{\alpha}_j \cdot \mathbf{p}_j + (\beta_j - 1)c^2 + V(r_j)] + \sum_{j < k} \frac{1}{r_{jk}}, \quad (25)$$

where $\boldsymbol{\alpha}$ and β are the Dirac matrices and p is the momentum operator. The electrostatic electron-nucleus interaction $V(r_j)$ has been generated from a two-parameter Fermi nuclear charge distribution (13). The effects of the Breit interaction, as well as QED effects, were neglected since they are expected to be small at the level of accuracy attainable in the present calculations.

B. Energy functionals

Several different methods of wave-function generation were employed in order to test the dependence of the calculated atomic EDMs on options available in the GRASP2K [10] implementation of the MCDHF method. One option is related

single-particle reduced matrix element $[n_a \kappa_a \| \hat{t}^k \| n_b \kappa_b]$ in expansion (7) for the operator of the electron EDM interaction with a magnetic field of a nucleus can be factorized into a reduced angular matrix element and a radial integral

to the variational energy functional in the wave-function optimization procedure. Two general forms of the energy functional are implemented in the GRASP2K [10] package.

1. Extended optimal level

One-electron orbitals based on the extended optimal level (EOL) form are optimized to minimize the energy functional, which is defined through Eq. (39) in Ref. [16], where generalized weights [Eq. (40) in Ref. [16]] determine a specific ASF (or a set of ASFs). Consequently, the orbitals in the EOL approach are optimal for a specific ASF or a set of ASFs.

2. Extended average level

One-electron orbitals based on the extended average level (EAL) form are optimized to minimize the (optionally weighted) sum of energies of all ASFs that may be constructed from a given set of CSFs, so eventually it yields an (optionally weighted) average energy of a set of atomic states. This approach is computationally much cheaper, but usually less accurate than the approach based on the EOL functional.

C. Virtual orbital sets

The numerical wave functions were obtained independently for the two parities. The calculations proceeded in two phases. Spectroscopic (occupied) orbitals were obtained in the Dirac-Hartree-Fock approximation. They were kept frozen in all subsequent calculations. Then virtual (correlation) orbitals were generated in several consecutive steps. At each step the virtual set has been extended by one layer of virtual orbitals. A *layer* is defined as a subset of virtual orbitals, usually with different angular symmetries, optimized simultaneously in one step, and usually frozen in all subsequent steps. In the present paper up to five layers of virtual orbitals of each of the s , p , d , f , and g symmetries were generated. At each stage only the outermost layer is optimized and the remaining orbitals (spectroscopic as well as other virtual layers) are kept frozen. Virtual orbitals were generated in an approximation in which all single and restricted double substitutions from valence orbitals and a subset of core orbitals to subsequent layers of virtual orbitals were included. The restriction was applied to double substitutions in such a way that only one electron was substituted from core shells; the other one had to be substituted from the valence shells (i.e., from the $7s$ shell in the case of

TABLE I. Contributions to the atomic EDM from TPT, PSS, SM, and electron EDM interactions, calculated for ^{225}Ra , using orthogonal (Orth) and nonorthogonal (Nonorth) orbital sets. The number for the VOS in the first column is the number of virtual orbital layers. Transition energies are experimental.

VOS	TPT		PSS		SM		$e\text{EDM}$	
	Orth	Nonorth	Orth	Nonorth	Orth	Nonorth	Orth	Nonorth
0 (DF)	-16.3	-15.81	-59.7	-57.87	-6.53	-6.32	-55.6	-46.67
1	-14.5	-15.51	-53.3	-57.09	-6.28	-7.01	-48.1	-43.69
2	-18.8	-19.90	-69.0	-72.95	-7.79	-8.16	-63.5	-58.07
3	-19.9	-20.68	-70.3	-75.83	-8.27	-8.59	-66.9	-60.13
4		-20.28		-74.42		-8.63		-58.45

the even-parity ground state of radium atom, $7s$ and $7p$ shells in the case of the odd-parity excited states of radium, and $6s$ and $6p$ in the cases of mercury and ytterbium). Five layers of virtual orbitals were generated for Hg and four layers for Ra and Yb. The combined contribution of the $n = 3$ shells to the hyperfine constants of the $7s7p\ ^1P$ state was evaluated in a previous paper [18] and found to be negligible, while the combined contribution of the $n = 4$ shells was below the 1% level. Therefore, in the present calculations the innermost core orbitals $1s$, $2s$, $2p$, $3s$, $3p$, and $3d$ of the radium atom were kept closed for electron substitutions. All other core orbitals, as well as valence orbitals, were subject to electron substitutions. By a similar argument, the innermost core orbitals $1s$, $2s$, and $2p$ of Hg and Yb were kept closed for electron substitutions. The reader is referred to Refs. [18,19] for further details of wave-function generation.

D. Nonorthogonal orbital sets

The matrix elements of all interactions were calculated between the ground state ns^2 ($J = 0$) and excited states with total angular momentum $J = 1$ and opposite parity for ^{225}Ra , ^{199}Hg , and ^{171}Yb . In principle, the optimal wave functions for calculations of EDM matrix elements are obtained in the extended optimal level form (see Sec. III B 1 above) separately for each parity. The wave functions optimized separately for the ground and excited states are built from independent sets of one-electron orbitals. The two sets are mutually nonorthogonal and they automatically account for relaxation effects involved in calculations of matrix elements between different atomic states [11,20]. On the other hand, the transition energies obtained from wave functions based on separately optimized orbital sets may be less accurate than transition energies obtained from calculations based on a common set of mutually orthogonal one-electron orbitals. The above situation often arises when multiconfiguration expansions are tailored specifically to include only those electron correlation effects that are important for one-electron expectation values. For one-electron matrix elements involved in the present calculations the dominant contributions arise from single and restricted double substitutions. We have not included the unrestricted double substitutions, i.e., the electron correlation effects with dominant contributions to the total energy, as well as higher-order substitutions, since their impact on EDMs is indirect and usually small [21].

We evaluated the effect of the relaxation of the wave functions by performing two parallel sets of calculations based on a common orbital set (orthogonal) and on two separately optimized orbital sets (nonorthogonal), respectively. Table I lists the atomic EDM for ^{225}Ra , calculated in several approximations. The first line [with the entry 0 (DF) in the first column] lists the results obtained with uncorrelated Dirac-Fock wave functions. The following lines provide the results obtained with different numbers (1–4) of virtual orbital layers included in the virtual orbital set (VOS). The number of virtual orbital layers in a given VOS is quoted in the first column. We skipped the orthogonal calculation with four virtual orbital layers since the preceding lines show clearly that the effects of nonorthogonality (i.e., the relaxation of wave functions) are of the order of a few percent, up to 11% for the interaction of the electron electric dipole moment with the nuclear magnetic field (the $e\text{EDM}$ entry in Table I).

The calculation of matrix elements in the nonorthogonal case requires a transformation of one-electron orbitals from which the wave functions of ground and excited states are built. The program BIOTRA2 [10] was applied to transform both wave functions to a biorthonormal form [22,23], which then permits one to use standard Racah algebra in evaluation of matrix elements.

E. Extended optimal level calculations

The final values of atomic EDMs, presented in the Tables IV–VII, were obtained with the extended optimal level optimization procedure described in Sec. III B 1 above. At each stage of generation of virtual orbital sets, a decision had to be made with respect to the number of atomic levels included in the variational energy functional. Table II presents the contributions $d_{\text{at}}^{\text{TPT}}$ to the atomic EDM of ^{225}Ra from the tensor-pseudotensor interaction (11). The contributions from particular atomic states are listed in subsequent lines. The radial wave functions were optimized within the EOL procedure, with different numbers of EOLs: 4, 6, 8, 10, or 12 levels, as indicated in the column headings of Table II. These data were obtained with experimental transition energies quoted from the National Institute of Standards and Technology (NIST) Atomic Spectra Database (ASD) [24].

An inspection of the Table II (in particular, the first entry on the last line, sum all) indicates that the $d_{\text{at}}^{\text{TPT}}$ expectation value becomes stable when eight or more levels are included in the extended optimal level energy functional. Analogous

TABLE II. The $d_{\text{at}}^{\text{TPT}}$ contribution to the atomic EDM, calculated with the EOL method for the first VOS, using different numbers of optimized levels and experimental transition energies, in units of $10^{-20} C_T(\sigma_A)|e|$ cm, for ^{225}Ra . Numbers in square brackets represent powers of 10.

Levels	4	6	8	10	12
$7s7p^3P$	-5.00	-4.46	-4.63	-4.59	-4.63
$7s7p^1P$	-1.03[1]	-8.80	-8.70	-8.69	-8.57
$7s8p^3P$		0.39	0.30	0.33	0.44
$7s8p^1P$		-1.12	-0.96	-1.01	-1.24
sum $s-p$	-1.53[1]	-1.40[1]	-1.40[1]	-1.40[1]	-1.40[1]
$6d7p^3D$	2.53[-3]	-7.72[-4]	2.96[-2]	-9.30[-2]	-6.91[-2]
$6d7p^3P$	1.98[-1]	-3.08[-2]	-1.13[-1]	3.55[-2]	7.34[-2]
sum $s-d$	2.00[-1]	-3.16[-2]	-8.33[-2]	-5.75[-2]	4.25[-3]
$s-p + s-d$	-1.51[1]	-1.40[1]	-1.41[1]	-1.41[1]	-1.40[1]
$6d8p^3D$			-4.79[-2]	-9.44[-3]	-3.63[-3]
$6d8p^3P$			-1.15[-1]	-4.90[-2]	-8.36[-2]
$7p8s^3P$				-1.96[-2]	-2.20[-2]
$7p8s^1P$				-6.02[-3]	-6.31[-3]
$6d7p^1P$					-5.12[-3]
$8s8p^3P$					1.50[-3]
sum D			-1.63[-1]	-8.41[-2]	-1.19[-1]
sum all	-1.51[1]	-1.40[1]	-1.42[1]	-1.41[1]	-1.41[1]

decisions were made for all virtual orbital sets, as well as for the other two elements. The final calculations were made with varying numbers of EOLs, between 2 levels for uncorrelated Dirac-Fock wave functions, with 6–8 levels in most correlated calculations, and up to 13 levels in one case.

F. Orbital contributions

Another interesting conclusion arises from the analysis of contributions of particular one-electron orbitals generated in the EOL optimization procedure. The analysis presented in Table II was made with only one virtual orbital layer because the extended optimal level optimization procedure described in Sec. III B 1 above becomes unstable with the increasing numbers of virtual layers and EOLs. However, already at this level of approximation the dominant contributions come from the singlet $7s7p^1P_1$ and triplet $7s7p^3P_1$ excited states. The states $7s8p^1P_1$ and $7s8p^3P_1$, involving the $8p$ orbital, contribute 9% and 3%, respectively (and their contributions partially cancel due to different signs). All other states contribute less than 1% each. The following lines present contributions of singlet and triplet states generated by single or double electron substitutions from the reference configuration $7s7p$ to the lowest available orbitals $8s$, $8p$, and $6d$. The line with the first entry sum $s-p$ shows the contributions of the four dominant states generated by single electron substitutions from the reference configuration. The line with the first entry sum $s-d$ shows the sum of entries from the preceding two lines of the $6d7p$ configuration; the line with the first entry $s-p+s-d$ shows the sum of all preceding contributions. The next six lines present the contributions of higher-lying levels and the line with the first entry sum D show the sum of the contributions from these six preceding lines. The last line, with the first entry sum all, shows the total sum of all contributions of all states listed in the preceding lines. We present the partial sums ($s-p$, $s-d$, $s-p+s-d$, and sum D) to show their dependence on the

number of EOLs. The contributions of individual levels are not very stable and in particular the small contributions may vary significantly, but the partial sums are more stable and the total sum (sum all) is strongly stabilized by the contributions from the dominant states.

It is interesting to make a comparison of Table II with Table VI from Ref. [25]. In Ref. [25] the contributions from $7s_{1/2}-7p_{1/2}$ and $7s_{1/2}-8p_{1/2}$ single-particle matrix elements (pairings in their language) are of comparable sizes, -324.468 and -306.133 , respectively, while in our calculations the relative sizes of the contributions from $7s_{1/2}-8p_{1/2}$, with respect to the contribution from the $7s_{1/2}-7p_{1/2}$ pairing, are 9% and 3% for singlet and triplet states, respectively. Also, there are differences with respect to the contributions of higher-symmetry orbitals. For instance, the contribution from $d_{5/2}$ orbitals is of the order of 4% (see Table VII in Ref. [25]), while in our calculations the contributions from $d_{5/2}$ orbitals are below 1%.

It is difficult to explain these differences, but one possible explanation is due to differences in optimization procedures and radial shapes of one-electron orbitals that resulted from these procedures, as discussed in Sec. III E. Different compositions of particular atomic states are likely consequences of differences in radial bases. The authors of Ref. [25] used Gaussian basis sets, while in our calculations we use numerical orbitals defined on a grid. We do not have insight into the details of the calculations presented in Ref. [25], but their Gaussian basis sets are likely to be evenly distributed over the entire configurational space.

Different theories use different methods of construction for atomic states. A consequence of these differences is the fact that comparisons of contributions from particular atomic states or from individual one-electron orbitals are not meaningful. All excited and virtual orbitals generated in our calculations were optimized with multiconfiguration expansions designed for valence and core-valence electron correlation effects,

resulting in virtual orbital shapes with maximal overlaps with valence and outer core spectroscopic orbitals. Consequently, the correlation corrections to the wave function are likely to be larger for the lower states included in the extended optimal level procedure. We performed comparison calculations with virtual orbitals generated with three different methods: the extended average level procedure, as described in Sec. III B 2; virtual orbitals generated within the screened hydrogenic approximation; and virtual orbitals from the Thomas-Fermi potential. As described in Sec. III B 2, one-electron virtual orbitals generated with the EAL functional are optimized to minimize the sum of energies of all states. Hydrogenic and Thomas-Fermi virtual orbitals are not variationally optimized; they just form orthogonal bases. Our comparison calculations indicate that calculations based on extended average level, hydrogenic, and Thomas-Fermi virtual orbitals converge slower than extended optimal level calculations and the contributions of higher-lying levels are larger compared to EOL results.

G. Transition energies

The summation in Eq. (4) runs over all excited states of appropriate parity and symmetry. The contributions of higher-lying levels are gradually decreasing since they are suppressed both by the energy denominators and by decreasing values of electric dipole matrix elements, as well as by decreasing overlaps of one-electron radial orbitals, entering integrals in Eqs. (14), (19), (21), and (23). In numerical calculations they have to be cut off at certain level of accuracy. Except where indicated otherwise, the results presented in the present paper were computed with experimental transition energies in the denominators of the matrix elements in Eq. (4). The transition energies were calculated from the NIST ASD database [24] and we included levels up to $6d7p^3P_1$ for ^{225}Ra , $6s8p^1P_1$ for ^{171}Yb , and $6s9p^1P_1$ for ^{199}Hg . However, several levels are missing in [24], so we employed an approach where those transition energies that were not available were replaced by the energies calculated with one of the three different methods: (i) using theoretical energies obtained from the MCDHF approach, (ii) with the energy of the upper level replaced by the energy of the lowest excited state, or (iii) with the energy of the upper level replaced by the experimental ionization limit. The choice was made between the above three options in the case of each missing level, based on the availability of a reliable theoretical energy or alternatively on the proximity of the lowest excited state or the experimental ionization limit. To verify this approach we performed test calculations where all three choices were used together. Table III presents the contributions from the tensor-pseudotensor interaction to the atomic EDM of radium isotope ^{225}Ra . Transition energies in Table III were taken from the MCDHF relativistic self-consistent-field (RSCF) calculation (column heading RSCF), MCDHF relativistic configuration-interaction (RCI) calculation (column heading RCI), experimental data (Expt.), experimental ionization limit (Expt. IL), and experimental energy of the lowest excited level (Expt. 1). The MCDHF RSCF case was a self-consistent-field Extended Optimal Level calculation, with 2, 7, 6, 8, and 6 EOL levels for DF, 1, 2, 3, and 4 VOS, respectively. The MCDHF RCI case was a configuration-interaction calculation with

TABLE III. Tensor-pseudotensor interaction contributions to the EDM for ^{225}Ra , in units of $10^{-20}C_T\langle\sigma_A\rangle|e|\text{cm}$, calculated with the EOL method and compared with data from other methods. Transition energies are taken from MCDHF RSCF calculation (RSCF), experimental data (Expt.), the MCDHF RCI calculation (RCI), the experimental ionization limit (Expt. IL), experimental value of lowest excited level (Expt. 1) (see the text for explanation). The number for the VOS in the first column is the number of virtual orbital layers.

VOS	^{225}Ra				
	RSCF	RCI	Expt.	Expt. IL	Expt. 1
0 (DF)	-18.31	-18.31	-15.81	-15.81	-15.81
1	-10.37	-11.81	-15.51	-14.70	-13.92
2	-12.04	-12.58	-19.90	-20.08	-20.45
3			-20.68	-21.22	-22.52
4			-20.28	-21.16	-22.32
Ref. [13] (DHF)					-3.5
Ref. [13] (CI+MBPT)					-17.6
Ref. [13] (RPA)					-16.7
Ref. [25] (CPHF)					-16.585

100 levels included. Their differences indicate the deviation incurred when the number of EOLs is varied. It should be noted that experimental values of the energies of the $7s7p$ levels were used in all cases in columns Expt., Expt. IL, and Expt. 1. The lowest $nsnp$ levels yield the largest contributions to all EDM matrix elements in the present calculations and their energies are available for all elements in question; therefore, replacements were made only for higher-lying levels. The number for the VOS in the first column of Table III represents the number of virtual orbital layers. These data indicate the sizes of errors, which may arise from replacing experimental transition energies with the experimental ionization limit (Expt. IL) or the experimental energy of the lowest excited level (Expt. 1). As can be seen, the deviation is less than 10% in the case of radium. The deviations of the data obtained with calculated transition energies are larger due to the nature of the wave functions built from nonorthogonal orbital sets, as explained in Sec. III D above.

H. Summation over excited states

As mentioned in Sec. III G above, the summation in Eq. (4) runs over all excited states of appropriate parity and symmetry. In numerical calculations the summation has to be truncated at finite number of terms and in the present paper up to five terms of each symmetry are explicitly evaluated. The contribution of the remaining part of the sum may be estimated by extrapolation. Let us consider as an example the contributions from the Rydberg series of the triplet states $6snp^3P_1$ of ^{199}Hg . After explicit numerical calculation of large contributions arising from low values of principal quantum number n , the contributions of higher-lying states entering the sum in Eq. (4) may be evaluated from the asymptotic behavior of the matrix elements in the numerator and of the transition energy in the denominator. The electric dipole matrix element

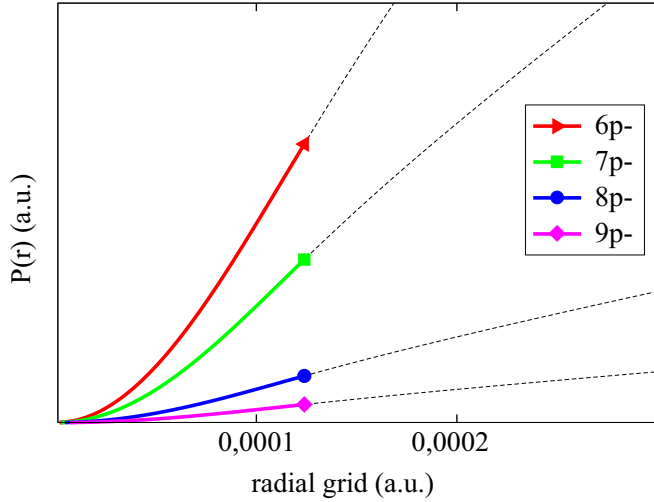


FIG. 1. (Color online) Large components $P(r)$ of the one-electron np radial orbitals of the triplet states $6snp\ ^3P_1$ ($n = 6, 7, 8, 9$) of ^{199}Hg . The solid line (colored) sections represent the radial shapes of the orbitals inside the ^{199}Hg nucleus. The $P(r)$ are in arbitrary units and the radial grid is in atomic units. See the text for further details.

scales with principal quantum number n as [26,27]

$$(E_0 - E_n) \langle 0 | \hat{D}_z | 6snp\ ^3P_1 \rangle^2 \sim (n^*)^{-3}, \quad (26)$$

where n^* is the effective quantum number of the running np electron in the series $6snp\ ^3P_1$, i.e., $n^* = n - \delta$, δ being the quantum defect (for the series $6snp\ ^3P_1$ of ^{199}Hg the quantum defect $\delta = 4.293$). The calculations of the matrix elements of the \mathcal{PT} -odd interactions involve radial integrals of atomic one-electron orbitals and all these integrals include factors in the integrands, which effectively cut off the integrals outside the nucleus [see Eqs. (14), (19), (21), and (23)]. Therefore, the dominant contribution to each integral comes from within or in the vicinity of the nucleus. The Dirac equation near the origin has a power-series solution and the n dependence near the origin is as follows [28–30]:

$$P(r) \sim (n^*)^{-3/2}, \quad (27)$$

$$Q(r) \sim (n^*)^{-3/2}, \quad (28)$$

where $P(r)$ and $Q(r)$ are large and small components of radial wave functions, respectively. Figure 1 shows the numerical large components $P(r)$ of the one-electron np radial orbitals, in the vicinity of the nucleus, for $n = 6, 7, 8, 9$, extracted from the triplet states $6snp\ ^3P_1$ in ^{199}Hg . The solid line (colored) sections represent the radial shapes of the orbitals inside the ^{199}Hg nucleus. The solid line sections of these components are monotonic and scale with n^* approximately as in Eq. (27). The small components $Q(r)$ scale similarly. (In the vicinity of the nucleus the amplitudes of the small components are large compared to the amplitudes of the large components.) Therefore, the integrands in the matrix elements of the \mathcal{PT} -odd interactions considered in this paper also scale with n^* of the running np electron as

$$\langle 6snp\ ^3P_1 | \hat{H}_{\text{int}} | 0 \rangle \sim (n^*)^{-3/2}. \quad (29)$$

The energy denominator in Eq. (4) saturates at the ionization energy for large- n values along the Rydberg series; therefore,

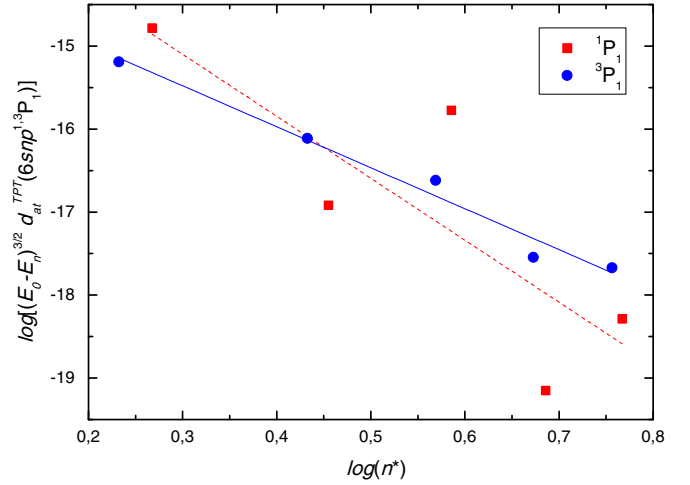


FIG. 2. (Color online) Tensor-pseudotensor interaction contributions to the atomic EDM in ^{199}Hg , multiplied by the energy denominators, as a function of the effective quantum number n^* of the np orbitals ($n = 6, 7, 8, 9, 10$) from the triplet $6snp\ ^3P_1$ (blue solid line with circles) and the singlet $6snp\ ^1P_1$ (red dashed line with squares) individual states of ^{199}Hg . See the text for further details.

the overall n dependence of subsequent terms in the sum in Eq. (4) involves a product of right-hand sides of Eqs. (26) and (29), which together yield the contribution from a particular $6snp\ ^3P_1$ state $d_{\text{at}}^{\text{int}}(6snp\ ^3P_1) \sim (n^*)^{-3}$. Eventually, the infinite sum in Eq. (4) may be evaluated in the following way. The first four terms are explicitly calculated from the numerical wave functions. The upper bound on the remaining terms is approximately evaluated by the Riemann ζ function. The relative correction, i.e., the contribution from the trailing terms (called the Riemann ζ tail) divided by the contribution from the four leading terms, is of the order of 1.5%, again with the assumption that the energy denominators saturated at the ionization energy. With the above assumption lifted, the relative correction would be smaller than 1.5% since the presence of the energy denominators increases the relative weights of the leading terms. The matrix elements in Eqs. (26) and (29) can be either positive or negative and not infrequently change sign partway up a series. Sign changes would of course decrease the relative correction mentioned above.

In order to validate the above reasoning we perform a separate calculation for ^{199}Hg , where singlet $6snp\ ^1P_1$ and triplet $6snp\ ^3P_1$ states of ^{199}Hg are separately generated for $n = 6, 7, 8, 9, 10$. Let us consider the contribution $d_{\text{at}}^{\text{TPT}}(6snp\ ^3P_1)$ to the total atomic EDM from the individual $6snp\ ^3P_1$ triplet state, i.e., from one term of the sum on the right-hand side of Eq. (4). When both sides of this equation are multiplied by the energy denominator, what remains on the right-hand side scales with $(n^*)^{-3}$ of the running np electron:

$$\begin{aligned} d_{\text{at}}^{\text{TPT}}(6snp\ ^3P_1)(E_0 - E_n)^{3/2} \\ = 2 \langle 0 | \hat{D}_z | 6snp\ ^3P_1 \rangle \langle 6snp\ ^3P_1 | \hat{H}_{\text{TPT}} | 0 \rangle \sim (n^*)^{-3}. \end{aligned} \quad (30)$$

Figure 2 shows the relation (30) in log-log coordinates obtained for the triplet $6snp\ ^3P_1$ and the singlet $6snp\ ^1P_1$ ($n = 6, 7, 8, 9, 10$) states of ^{199}Hg . The straight-line linear fits yield the slope -4.6 for the triplet $6snp\ ^3P_1$ state (blue solid line with circles) and -7.3 for the singlet $6snp\ ^1P_1$ state

(red dashed line with squares). Both slope values should be compared to -3.0 obtained from the considerations presented in the preceding paragraphs. Analogous linear fits for other Rydberg series of all three elements ^{225}Ra , ^{199}Hg , and ^{171}Yb and for all four \mathcal{PT} -odd interactions yield the slopes in the range from -3.9 to -9.1 . The singlet series exhibit larger slope values compared to the triplet series. The large values of the slope, the large range of slope values, and noticeable deviations from linear fits reflect the fact that the slopes are fitted to the calculated data obtained from the leading terms in Eq. (4), corresponding to the lowest atomic levels of a particular Rydberg series. The lowest levels of a Rydberg series are not truly Rydberg-like in the sense that the valence electrons are not yet completely screened by the electronic core and they exhibit strong deviations from Rydberg regularities, due to interelectronic interactions.

Eventually, the upper bounds on the trailing terms in all cases were evaluated by partial summation of Riemann ζ function. Based on these analyses, we concluded that the first four terms of each Rydberg series in Eq. (4) yield 98% or more of the series' contribution to the total atomic EDMs of all three elements ^{225}Ra , ^{199}Hg , and ^{171}Yb , and for all four \mathcal{PT} -odd interactions.

I. Uncertainty estimates

Estimates of uncertainty in *ab initio* calculations are far more difficult and uncertain than the calculations themselves, particularly in situations where an atomic property is evaluated, which has not been calculated before within the same approach for any other element. We can indicate possible sources of uncertainties, but their sizes are difficult to estimate. The possible sources of uncertainties are the following.

1. Electron correlation effects

In extensive large-scale calculations the relative accuracy can reach 1%–5%, depending on the expectation value in question (see, e.g., [18,19]). An estimate of uncertainty associated

TABLE IV. Tensor-pseudotensor interaction contributions to the EDM, calculated with the EOL method in different virtual sets, in units of $10^{-20}C_T(\sigma_A)|e|$ cm, for ^{225}Ra , ^{199}Hg , and ^{171}Yb , compared with data from other methods.

VOS	^{225}Ra		^{199}Hg	^{171}Yb	
	Expt.	Expt. IL	Expt. 1	Expt.	Expt.
0 (DF)	-15.81	-15.81	-15.81	-6.15	-3.31
1	-15.51	-14.70	-13.92	-4.86	-1.94
2	-19.90	-20.08	-20.45	-5.70	-3.71
3	-20.68	-21.22	-22.52	-6.10	-4.03
4	-20.28	-21.16	-22.32	-5.53	-4.24
Ref. [13] (DHF)	-3.5			-2.4	-0.70
Ref. [31] (DHF)				-2.0	
Ref. [13] (CI+MBPT)	-17.6			-5.12	-3.70
Ref. [13] (RPA)	-16.7			-5.89	-3.37
Ref. [31] (RPA)				-6.0	
Ref. [32] (RPA)				-6.75	
Ref. [25] (CPHF)	-16.585				-3.377
Ref. [33] (CCSD)				-4.3	

TABLE V. Pseudoscalar-scalar interaction contributions to the EDM, calculated with the EOL method in different virtual sets in units of $10^{-23}C_P(\sigma_A)|e|$ cm for ^{225}Ra , ^{199}Hg , and ^{171}Yb , compared with data from other methods.

VOS	^{225}Ra	^{199}Hg	^{171}Yb
0 (DF)	-57.87	-21.49	-10.84
1	-57.09	-17.16	-6.31
2	-72.95	-19.94	-12.20
3	-75.83	-21.53	-13.26
4	-74.42	-19.45	-13.94
Ref. [13] (DHF)	-13.0	-8.7	-2.4
Ref. [13] (CI+MBPT)	-64.2	-18.4	-12.4
Ref. [13] (RPA)	-61.0	-20.7	-10.9

with the electron correlation effects can be obtained in several ways. In the limit of a very large number of virtual orbital layers an estimate of uncertainty may be related to oscillations of the calculated expectation value plotted as a function of the size of the multiconfiguration expansion [19]. In the present paper an estimate of the uncertainty was based on the differences between the data obtained with the largest two multiconfiguration expansions, represented by three and four layers of virtual orbitals in Tables IV–VII. We abstained from extending the virtual sets beyond the fourth layer because there are several other possible sources of uncertainty in the present calculations. An inspection of the tables indicates that the differences between the last two lines range between 0.47% for the Schiff moment of Ra and 15.77% for the Schiff moment of Hg (Table VI). We may assume the latter as an estimate of uncertainty associated with the neglected electron correlation effects.

2. Wave-function relaxation

As explained in Sec. III D, the effects of wave-function relaxation were partially accounted for in the present calculations by using nonorthogonal orbital sets for opposite parities. An inspection of Table I indicates that the uncertainty that may arise from wave-function relaxation effects is of the order of 10%, although this estimate is based on relaxing only the ASF

TABLE VI. Schiff moment contributions to the atomic EDM, calculated with the EOL method in different virtual sets, in units of $10^{-17}[S/(|e| \text{fm}^3)]|e|$ cm, for ^{225}Ra , ^{199}Hg , and ^{171}Yb , compared with data from other methods.

VOS	^{225}Ra	^{199}Hg	^{171}Yb
0 (DF)	-6.32	-2.46	-1.54
1	-7.01	-2.45	-0.88
2	-8.16	-2.23	-1.83
3	-8.59	-2.98	-2.05
4	-8.63	-2.51	-2.15
Ref. [13] (DHF)	-1.8	-1.2	-0.42
Ref. [13] (CI+MBPT)	-8.84	-2.63	-2.12
Ref. [13] (RPA)	-8.27	-2.99	-1.95
Ref. [34] (CI+MBPT)	-8.5	-2.8	
Ref. [35] (TDHF)		-2.97	-1.91
Ref. [33] (CCSD)		-5.07	

TABLE VII. Contributions of the electron EDM interaction with a magnetic field of nucleus to the atomic EDM are calculated with the EOL method in different virtual sets, in units of $d_e \times 10^{-4}$, for ^{225}Ra , ^{199}Hg , and ^{171}Yb , compared with data from other methods.

VOS	^{225}Ra	^{199}Hg	^{171}Yb
0 (DF)	-46.67	13.41	5.37
1	-43.69	9.58	3.17
2	-58.07	12.22	5.72
3	-60.13	12.80	6.09
4	-58.45	11.45	6.44
Ref. [13] (DHF)	-11	4.9	1.0
Ref. [36] (DHF)		5.1	
Ref. [13] (CI+MBPT)	-55.7	10.7	5.45
Ref. [13] (RPA)	-53.3	12.3	5.05
Ref. [36] (RPA)		13	

wave function of the ground state on the one hand and the ASF wave functions of all excited states taken together on the other. A more general albeit far more expensive approach would be to generate separate atomic state functions for the ground state, as well as for each excited state, implying nonorthogonality between all ASFs of both parities.

3. Energy denominators

As discussed in Sec. III G, the summation in Eq. (4) runs over all excited states of appropriate parity and symmetry. The NIST ASD [24] is of course finite; therefore, several levels with unknown energies had to be included in the present calculations. The uncertainty that may arise due to replacements described in Sec. III G should not exceed 10% in the case of the radium atom and we expect the same order of magnitude in the case of ytterbium and mercury.

4. Systematic errors

The possible sources of systematic errors include neglecting the contribution of the core excitations to the sum over states (4); truncation of the summation in Eq. (4); contribution of the continuum in Eq. (4); omission of double, triple, and higher-order substitutions; the effects of the Breit interaction; and QED effects. Because of the singular nature of the \mathcal{P} -odd and \mathcal{PT} -odd operators, the contribution of the core excitations to the sum (4) can be quite large and tends to decrease the final result. Table VII in Ref. [13] shows the core contributions, of the order of 10%–20%, for each of the three elements of interest (Yb, Hg, and Ra) with opposite sign with respect to the final result. The upper bound on the sum of the trailing terms in Eq. (4) was evaluated in Sec. III H above and it is less than 2%. The contribution of the continuum is difficult to estimate since it is partially accounted for by the virtual set. In the present paper we neglected the explicit summation over the continuum, we assumed that the continuum spectrum contribution may be included into the error budget, and we computed only the contribution of the bound states. The calculations of EDMs involve radial integrals of atomic one-electron orbitals and all these integrals include factors in the integrands, which effectively cut off the integrals outside the nucleus, so the contribution to the integral comes from within or in the vicinity of the nucleus. Therefore, an estimate of systematic errors due

to multiple electron substitutions can be made by comparing the EDM calculations with hyperfine-structure calculations, where an integrand in the form r^{-2} appears in a one-electron integral, which in turn renders the dominant contribution from the first half of the radial orbital oscillation, i.e., near the nucleus. In certain cases in the hyperfine-structure calculations the effects of double and triple substitutions can be quite sizable, of the order of 10%–20%, but they often partly cancel and the net deviation is often smaller than 10% [37,38]. The effects of quadruple and higher-order substitutions are negligible. The effects of the Breit interaction and QED are usually of the order of 1%–2% or less for neutral systems.

5. Error budget

Based on the above estimates, the relative root-mean-square deviation of the present calculations yields $\sigma = 25\%$.

IV. FINAL RESULTS, DISCUSSION, AND OUTLOOK

A. Summary

Atomic EDMs arising from \mathcal{PT} -odd tensor-pseudotensor and pseudoscalar-scalar electron-nucleon interactions, the nuclear Schiff moment, and the interaction of the electron electric dipole moment with the nuclear magnetic field are presented in Tables IV–VII for the $J=0$ ground states of ^{225}Ra , ^{199}Hg , and ^{171}Yb . The matrix elements and atomic EDMs were calculated using recently developed programs in the framework of the GRASP2K code [10]. One of the objectives of the present calculations was to test these programs. Therefore, the results are compared with the data obtained by other methods: random-phase approximations (RPAs), many-body perturbation theory and configuration-interaction (CI+MBPT), coupled-cluster single-double theory (CCSD) technique, and coupled perturbed Hartree-Fock (CPHF) theory. These methods are usually more accurate in calculations of properties of closed-shell atoms. We should mention that in Tables IV–VII we quoted the final results from Ref. [13], corresponding to the CI+MBPT method, as well as their intermediate results, corresponding to the Dirac-Hartree-Fock (DHF) and RPA methods. A similar distinction applies to the RPA and DHF methods in Refs. [31,36].

An inspection of the tables indicates that the differences between our results and the data obtained with the above-mentioned methods [13,31,32,34–36] range between 1.5% for the Schiff moment of Ra (Table VI) and 22.1% for the tensor-pseudotensor interaction of Hg (Table IV), all of them within the error bounds estimated in Sec. III I 5 above. Despite the reasonable agreement at the level of the correlated calculations, very large differences should be noted at the uncorrelated levels: the DF approximation in our calculations and the DHF approximation in Refs. [13,36]. We used the different symbols to visually differentiate the results obtained with different numerical codes, but the DF and DHF approximations are formally identical within the Dirac-Fock theory and should yield similar values, within numerical accuracies of the Dirac-Fock codes. A possible explanation for these large differences may be the fact that in our (DF) calculations the summation in Eq. (4) runs over only the two lowest excited states, the singlet $nsnp\ ^1P$ and triplet $nsnp\ ^3P$, which are generated at the

Dirac-Fock level of the GRASP2K code [10]. On the other hand, in Refs. [13,36] the summation was probably carried over all excited states, which can be constructed from a suitable set of virtual orbitals. Otherwise, we do not have an explanation.

Large differences at the level of the correlated calculations should be noted between our results and the data obtained with the CPHF theory [25]. The differences are 18% for the TPT interaction of Ra and 39% for the TPT interaction of Hg (see Table IV). The largest disagreement appears to be between the result of the present calculations and the value obtained with the CCSD theory [33] for the Schiff moment of Hg (see Table VI). The difference amounts to 102%. It is difficult to explain some of the above-mentioned differences. They may be due to different orbital shapes and contributions, and relaxation effects, discussed in Secs. III F and III D, respectively.

Another objective of the present calculations was to test the methods of wave-function generation, as described in more detail in Sec. III A, and of multiconfiguration expansions designed to account for valence and core-valence electron correlation effects. The reasonably good agreement of our results with the data obtained within the RPA and CI+MBPT methods [13,31,32,34–36] seems to indicate that the multiconfigurational model employed in the present calculations accounts for the bulk of the electron correlation effects. With adequate computer resources, these calculations may be extended in the future and include also core-core electron correlation effects, as well as the contribution of the core excitations to the sum over states in Eq. (4). Based on the experiences with other atomic properties, as well as on the present EDM calculations, we expect that the accuracy of the EDM calculations may be improved by a factor of 10 with respect to the current relative root-mean-square deviation of the order of 25%.

B. Outlook

Several refinements are possible with respect to the methods used in the present paper. To account more accurately for the

electron relaxation, separate wave functions for the leading contributors to EDMs may be generated. A more general albeit far more expensive approach would be to generate separate ASFs for the ground state, as well as for each excited state, relaxing orthogonality of the orbital sets between all ASFs of both parities. The upper bound on the tail of the sum over bound states in Eq. (4) can be lowered by generating one or more virtual orbital layers. The evaluation of the sum in Eq. (4) over the continuum part of the spectrum can in principle be carried out fully numerically.

The expectation values $d_{\text{at}}^{\text{int}}$ were calculated with theoretical (if reliable) and experimental (if available) transition energies, as explained in Sec. III G. In fully correlated calculations theoretical transition energies would have to be evaluated with all single and unrestricted double substitutions. They would be computationally much more expensive than those presented in the present paper, but possible with the currently available massively parallel computers. Electron correlation effects can also be accounted for using the partitioned correlation function interaction method [39], which allows contributions from single and unrestricted double substitutions deep down in the atomic core to be summed up in a very efficient way. In the near future we should be able to perform fully *ab initio* calculations for atoms with arbitrary shell structures.

ACKNOWLEDGMENTS

The authors wish to thank the Visby program of the Swedish Institute for a collaborative grant. J.B. acknowledges support from the Polish Ministry of Science and Higher Education (MNiSW) in the framework of the scientific grant No. N N202 014140. The large-scale calculations were carried out with the supercomputer Deszno purchased through financial support of the European Regional Development Fund in the framework of the Polish Innovation Economy Operational Program (Contract No. POIG.02.01.00-12-023/08).

-
- [1] I. B. Khriplovich and S. K. Lamoreaux, *CP Violation Without Strangeness* (Springer, Berlin, 1997).
 - [2] W. C. Griffith, M. D. Swallows, T. H. Loftus, M. V. Romalis, B. R. Heckel, and E. N. Fortson, *Phys. Rev. Lett.* **102**, 101601 (2009).
 - [3] C. A. Baker, D. D. Doyle, P. Geltenbort, K. Green, M. G. D. van der Grinten, P. G. Harris, P. Jaydjiev, S. N. Ivanov, D. J. R. May, J. M. Pendlebury *et al.*, *Phys. Rev. Lett.* **97**, 131801 (2006).
 - [4] B. C. Regan, E. D. Commins, C. J. Schmidt, and D. DeMille, *Phys. Rev. Lett.* **88**, 071805 (2002).
 - [5] J. J. Hudson, D. M. Kara, I. J. Smallman, B. E. Sauer, M. R. Tarbutt, and E. A. Hinds, *Nature (London)* **473**, 493 (2011).
 - [6] T. A. C. J. Baron, W. C. Campbell, D. DeMille, J. M. Doyle, G. Gabrielse, Y. V. Gurevich, P. W. Hess, N. R. Hutzler, E. Kirilov, I. Kozyryev *et al.*, *Science* **343**, 269 (2014).
 - [7] J. S. M. Ginges and V. V. Flambaum, *Phys. Rep.* **397**, 63 (2004).
 - [8] *Advanced Series on Directions in High Energy Physics*, edited by B. L. Roberts and W. J. Marciano (World Scientific, Singapore, 2009), Vol. 20.
 - [9] V. A. Dzuba and V. V. Flambaum, *Int. J. Mod. Phys. E* **21**, 1230010 (2012).
 - [10] P. Jönsson, G. Gaigalas, J. Bieroń, C. Froese Fischer, and I. Grant, *Comput. Phys. Commun.* **184**, 2197 (2013).
 - [11] J. Bieroń, G. Gaigalas, E. Gaidamauskas, S. Fritzsche, P. Indelicato, and P. Jönsson, *Phys. Rev. A* **80**, 012513 (2009).
 - [12] G. Gaigalas, J. Bieroń, and L. Radžiūtė, *J. Phys.: Conf. Ser.* **488**, 122001 (2014).
 - [13] V. A. Dzuba, V. V. Flambaum, and S. G. Porsev, *Phys. Rev. A* **80**, 032120 (2009).
 - [14] I. P. Grant, *Relativistic Quantum Theory of Atoms and Molecules: Theory and Computation* (Springer, New York, 2007).
 - [15] G. Gaigalas, Z. Rudzikas, and C. Froese Fischer, *J. Phys. B* **30**, 3747 (1997).
 - [16] K. G. Dyall, I. P. Grant, C. T. Johnson, F. A. Parpia, and E. P. Plummer, *Comput. Phys. Commun.* **55**, 425 (1989).
 - [17] V. V. Flambaum and J. S. M. Ginges, *Phys. Rev. A* **65**, 032113 (2002).

- [18] J. Bieroń and P. Pyykkö, *Phys. Rev. A* **71**, 032502 (2005).
- [19] J. Bieroń, C. Froese Fischer, P. Indelicato, P. Jönsson, and P. Pyykkö, *Phys. Rev. A* **79**, 052502 (2009).
- [20] J. Bieroń, C. Froese Fischer, S. Fritzsche, and K. Pachucki, *J. Phys. B* **37**, L305 (2004).
- [21] B. M. Roberts, V. A. Dzuba, and V. V. Flambaum, *Phys. Rev. A* **89**, 042509 (2014).
- [22] P. Å. Malmqvist, *Int. J. Quantum Chem.* **30**, 479 (1986).
- [23] J. Olsen, M. R. Godefroid, P. Jönsson, P. Å. Malmqvist, and C. Froese Fischer, *Phys. Rev. E* **52**, 4499 (1995).
- [24] <http://www.nist.gov/pml/data/asd.cfm>
- [25] K. V. P. Latha and P. R. Amjith, *Phys. Rev. A* **87**, 022509 (2013).
- [26] R. D. Cowan, *The Theory of Atomic Structure and Spectra* (University of California Press, Berkeley, 1981), p. 436.
- [27] I. Ahmad, U. Griesmann, I. Martin, W. Dussa, M. A. Baig, and J. Hormes, *J. Phys. B* **29**, 2963 (1996).
- [28] I. B. Khriplovich, *Parity Nonconservation in Atomic Phenomena* (Gordon & Breach, New York, 1991).
- [29] I. B. Khriplovich and S. K. Lamoreaux, *CP Violation Without Strangeness* (Ref. [1]), p. 151.
- [30] I. P. Grant, *Relativistic Quantum Theory of Atoms and Molecules: Theory and Computation* (Ref. [14]), p. 148.
- [31] A.-M. Mårtensson-Pendrill, *Phys. Rev. Lett.* **54**, 1153 (1985).
- [32] K. V. P. Latha, D. Angom, R. J. Chaudhuri, B. P. Das, and D. Mukherjee, *J. Phys. B* **41**, 035005 (2008).
- [33] K. V. P. Latha, D. Angom, B. P. Das, and D. Mukherjee, *Phys. Rev. Lett.* **103**, 083001 (2009).
- [34] V. A. Dzuba, V. V. Flambaum, J. S. M. Ginges, and M. G. Kozlov, *Phys. Rev. A* **66**, 012111 (2002).
- [35] V. A. Dzuba, V. V. Flambaum, and J. S. M. Ginges, *Phys. Rev. A* **76**, 034501 (2007).
- [36] A.-M. Mårtensson-Pendrill and P. Öster, *Phys. Scr.* **36**, 444 (1987).
- [37] B. Engels, *Theor. Chim. Acta* **86**, 429 (1993).
- [38] J. Bieroń, C. Froese Fischer, P. Jönsson, and P. Pyykkö, *J. Phys. B* **41**, 115002 (2008).
- [39] S. Verdebout, P. Rynkun, P. Jönsson, G. Gaigalas, C. Froese Fischer, and M. Godefroid, *J. Phys. B* **46**, 085003 (2013).